ChemComm

COMMUNICATION

View Article Online
View Journal | View Issue

Check for updates

Cite this: *Chem. Commun.*, 2020, 56, 1964

Received 12th December 2019, Accepted 4th January 2020

DOI: 10.1039/c9cc09642f

rsc.li/chemcomm

Tuning the size of photo-deposited metal nanoparticles *via* manipulating surface defect structures of TiO_2 nanocrystals†

Xian Zhou,[a] Kun Qian,*[a] Yunshang Zhang,[a] Dan Li,[a] Zeyue Wei,[a] Huijuan Wang,[b] Run Ye,[c] Jiandang Liu,[c] Bangjiao Ye[c] and Weixin Huang*[a]

Here we report a new method for controlling photo-deposited metal nanoparticle size by manipulating surface defect structures of TiO_2 nanocrystals. Our results demonstrate that the isolated oxygen vacancy could serve as an electron trapper while the oxygen vacancy cluster could act as an electron–hole recombination site in the photo-deposition process.

The photo-deposition (PD) method has received great interest[1–5] since Kraeutler and Bard successfully obtained well-dispersed Pt nanoparticles on TiO_2 by illuminating a slurry of anatase powder together with Pt precursor.[6] Compared to other deposition processes, PD is easy to operate and control. Great efforts have been made to optimize the PD process and create effective catalytic materials, and impressive accomplishments have been achieved in the past decade. Zheng's group[7] reported a photochemical strategy to fabricate a stable atomically dispersed supported Pd on ultrathin TiO_2 nanosheets and believed that the adsorbed Pd complexes on the TiO_2 surface are responsible for the atomically dispersed Pd atoms. Chan and Barteau[8] prepared highly uniform photo-deposited Ag/TiO_2 and Au/TiO_2 catalysts by applying a fiber optic illuminator as a light source. Given that PD is an effective method to unveil the distribution of photo-generated charges in a photocatalytic system, Li's group[9] successfully synthesized Pt/MnO_x–$BiVO_4$ co-catalysts by selectively photo-depositing metallic Pt and MnO_x onto different $BiVO_4$ facets with different spatial charge distributions. They[10] further positioned the active sites of water oxidation using a similar method. We should notice that, nowadays, most studies on the influence of PD parameters are on the role of the sacrificial reagent,[11] the influence of the pH environment,[12] the stability of the metal precursor,[13] the influence of the light source and light intensity,[14] and the influence of spatial charge distributions.[9] However, the effects of surface structures, especially the roles of surface defects during the PD process, have not been adequately described. Specifically speaking, surface defects can serve as an electron trapper or charge recombination center, but scientists can only judge the influence of defects from comparing the photo-catalytic performances.[15,16] The relationship between defect structures and their specific role during the PD process is still indistinct.

In our previous study, anatase TiO_2 with different facets has been synthesized and detailed surface defect structures have been well identified,[17–20] which provides us with a great opportunity to figure out the particular roles of surface defects during the PD process. Herein, we synthesized anatase TiO_2 nanocrystals enclosed by {001} and {100} facets, in which two types of defect structures have been clarified by applying electron paramagnetic resonance (EPR) and *in situ* diffuse reflectance infrared Fourier transform spectroscopy (DRIFTS) study. We demonstrate that the defects on TiO_2{001} could serve as an electron trapper and facilitate the formation of small photo-deposited metal nanoparticles (such as Au, Pt, and Ag) while the defects on TiO_2{100} could not directly participate in the PD process and only result in large metal nanoparticles. Our results also show that both the intensity and the structure of the surface defects can be controlled by pretreating TiO_2 at high temperature, which provides a great opportunity to systematically synthesize photo-deposited metal nanoparticles with designed size distributions. These findings greatly broaden and deepen the understanding of the influence of surface defects on the photo-generated charge separation.

Fig. 1A and B display TEM images of the as-synthesized TiO_2{100} (A) and TiO_2{001} (B) nanocrystals. The morphologies of these nanocrystals are quite uniform. All these microscopic results agree with our previous results.[18] The BET-specific surface areas of TiO_2{100} and TiO_2{001} nanocrystals are 99

---

[a] *Hefei National Laboratory for Physical Sciences at the Microscale, Key Laboratory of Surface and Interface Chemistry and Energy Catalysis of Anhui Higher Education Institutes, CAS Key Laboratory of Materials for Energy Conversion, and Department of Chemical Physics, University of Science and Technology of China, Jinzhai Road 96, Hefei 230026, China. E-mail: qiankun@ustc.edu.cn, huangwx@ustc.edu.cn*

[b] *Engineering and Materials Science Experiment Center, University of Science and Technology of China, Jinzhai Road 96, Hefei 230026, China*

[c] *State Key Laboratory of Particle Detection and Electronics, University of Science and Technology of China, Jinzhai Road 96, Hefei 230026, China*

† Electronic supplementary information (ESI) available. See DOI: 10.1039/c9cc09642f

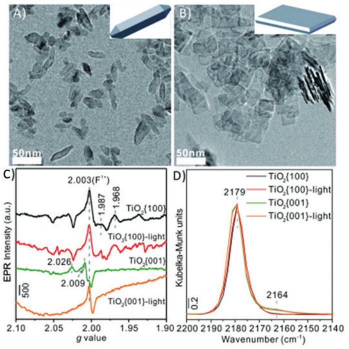

Fig. 1 TEM images of (A) TiO_2\{100\}, and (B) TiO_2\{001\}. (C) EPR spectra of various TiO_2 materials. (D) *In situ* DRIFTS spectra of CO chemisorption on various TiO_2 materials.

and 102 m^2 g^{-1}. The surface isoelectric points of TiO_2\{100\} and TiO_2\{001\} nanocrystals are pH 5.2 and 4.7 (Fig. S1, ESI†). The bandgap energies of TiO_2\{100\} and TiO_2\{001\} calculated from the UV-Vis spectra (Fig. S2, ESI†) are 3.02 eV for TiO_2\{100\} and 3.09 eV for TiO_2\{001\} (Fig. S3, ESI†).

The defect structures of the TiO_2 nanocrystals were characterized by EPR which is sensitive to species with unpaired electrons (Fig. 1C). TiO_2\{100\} and TiO_2\{001\} exhibit features of g = 2.026 arising from the O^{2-} species[21] and g = 2.003–2.009 arising from the oxygen vacancy (O_V) with a single electron (F^{1+}).[16] Two additional features of g = 1.987 and g = 1.968 respectively assigned to the subsurface/bulk ${Ti_{bulk}}^{3+}$ species and surface ${Ti_{surf}}^{3+}$ species[21,22] appear for TiO_2\{100\} but not for TiO_2\{001\}, which is consistent with our previous findings.[20] The EPR spectra of TiO_2 nanocrystals after light irradiation have also been applied to study the defect structures of TiO_2 under PD conditions. TiO_2\{100\} exhibits a similar EPR spectrum before and after light irradiation; in contrast, the peak assigned to O^{2-} species disappears and the peak F^{1+} becomes symmetrical in the EPR spectrum of TiO_2\{001\} after light irradiation. Although both TiO_2\{100\} and TiO_2\{001\} present a feature of g = 2.003 arising from the O_V with a single electron, the difference of symmetries of F^{1+} implies two types of defect structures. The symmetrical peak in TiO_2\{001\} is assigned to isolated O_V trapped one electron, while the unsymmetrical peak in TiO_2\{100\} is caused by the interaction of single-electron-trapped O_V and implies that O_V clusters exist in TiO_2\{100\}.[16,23] The surface structures of TiO_2 nanocrystals were further determined by applying adsorbed CO as a probe molecule. Fig. 1D shows *in situ* DRIFTS spectra of CO adsorption on TiO_2 nanocrystals with a CO pressure of 200 Pa at 123 K. Both TiO_2\{100\} and TiO_2\{001\} before and after light irradiation exhibit a vibrational band at 2179 cm^{-1} arising from CO adsorbed at Ti_{5c} sites of TiO_2.[17] A tailing peak at 2164 cm^{-1} arising from CO adsorbed at Ti sites of TiO_2 with partial negative charge has been observed only in TiO_2\{001\}, which is related to the isolated O_V on the TiO_2\{001\} surface.

Au/TiO_2 catalysts with calculated 0.2–3% Au/TiO_2 weight ratio were prepared by the PD method employing TiO_2\{100\} and TiO_2\{001\} as supports. The real Au loadings of Au/TiO_2 catalysts were analyzed by inductively coupled plasma atomic

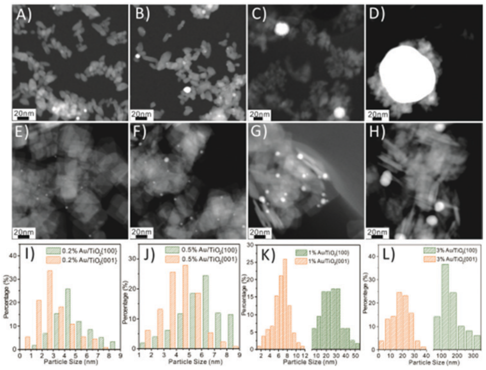

Fig. 2 HAADF-STEM images of various Au/TiO_2 catalysts with different Au loadings: (A–D) 0.2%, 0.5%, 1%, 3% Au/TiO_2\{100\}. (E–H) 0.2%, 0.5%, 1%, 3% Au/TiO_2\{001\}. (I–L) Size distributions of 0.2%, 0.5%, 1%, 3% Au/TiO_2.

emission spectroscopy (ICP-AES), and the results (Table S2, ESI†) indicate that Au real loadings are close to the calculated loadings. In the X-ray diffraction (XRD) patterns (Fig. S4, ESI†), all Au/TiO_2 catalysts only display diffraction patterns of anatase TiO_2 (JCPDS card no. 89-4921), and no diffraction peaks attributed to Au could be identified except for 3% Au/TiO_2\{100\} and 3% Au/TiO_2\{001\}. 3% Au/TiO_2\{100\} exhibits a much sharper Au(111) diffraction peak than 3% Au/TiO_2\{001\}, from which the calculated sizes of Au nanoparticles following the Scherrer formula are 18.3 and 7.5 nm in 3% Au/TiO_2\{100\} and 3% Au/TiO_2\{001\}.

Fig. 2 displays high-angle annular dark field (HAADF)-scanning transmission electron microscope (STEM) images and Au nanoparticle size distributions of various Au/TiO_2 catalysts. The Au nanoparticle size distributions in each catalyst were acquired by counting more than 100 Au nanoparticles. The average Au nanoparticle sizes are much more uniform and smaller in Au/TiO_2\{001\} catalysts than those in Au/TiO_2\{100\}, as shown in Table S2 (ESI†). Given that TiO_2\{100\} and TiO_2\{001\} exhibit a similar surface area, surface isoelectric point and band gap energy, the influence of precursor adsorption and light absorption capacity should not cause different size distributions of photo-deposited Au. We believe that the surface structures of TiO_2 nanocrystals, especially the defect structures, should affect the size distributions of photo-deposited Au nanoparticles.

We further applied an EPR study to investigate the defect structures of TiO_2 nanocrystals after photo-deposited Au nanoparticles. Fig. 3A and B display the EPR spectra of Au/TiO_2\{100\} and Au/TiO_2\{001\} with various photo-deposited Au loadings. No significant change of the EPR signal has been observed in Au/TiO_2\{100\} with increasing the amount of Au loading, while the EPR feature peak F^{1+} of TiO_2\{001\} rapidly disappears even after photo-depositing 0.2% Au. Our EPR results demonstrate that photo-deposited Au could interact with isolated O_V on the TiO_2\{001\} surface rather than O_V clusters on the TiO_2\{100\} surface, which is different from previous findings of deposited Au on TiO_2 nanocrystals *via* a deposition–precipitation (DP) method.[20] In our previous study, we found that both the O_V clusters on TiO_2\{100\} and isolated O_V on TiO_2\{001\} could serve as nucleation and growth sites of Au nanoparticles during the DP process, and TiO_2\{100\} with large numbers of defects can

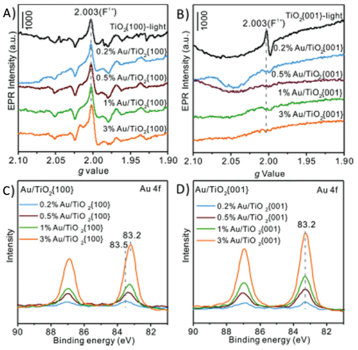

Fig. 3 (A and B) EPR spectra of (A) $TiO_2\{100\}$-light and $Au/TiO_2\{100\}$, (B) $TiO_2\{001\}$-light and $Au/TiO_2\{001\}$. (C and D) Au 4f XPS spectra of various Au/TiO_2 catalysts: (C) $Au/TiO_2\{100\}$, (D) $Au/TiO_2\{001\}$.

sustain much more dispersive deposited Au than $TiO_2\{001\}$ with fewer defects. Although the defects on both $TiO_2\{100\}$ and $TiO_2\{001\}$ could adsorb Au precursor and stabilize small Au nanoparticles during the thermal treatment, notably, only the isolated O_V on $TiO_2\{001\}$ could act as active sites for photo-deposited Au.

Positron annihilation lifetime spectroscopy (PALS) has been applied to investigate the structures of surface O_V (Fig. S5, ESI† and Table 1). We found that two types of τ_1 and τ_2 components respectively correspond to the annihilation of positrons in small and large O_V in TiO_2,[25] which is consistent with isolated O_V and O_V clusters in our EPR study. The ratio of isolated O_V in $TiO_2\{001\}$ is much higher than that in $TiO_2\{100\}$, suggesting that the isolated O_V mainly exist in $TiO_2\{001\}$ rather than $TiO_2\{100\}$. The τ_1 component assigned to isolated O_V disappears and a new τ_3 component with longer positron annihilation lifetime was observed after photo-depositing Au, which suggests that the isolated O_V should be the active site for the photo-deposition of Au and the interaction between Au and O_V could create a long lifetime component for positron annihilation.[26] Notably, PALS suggests that a large number of O_V clusters exist in $TiO_2\{001\}$ while we did not observe O_V clusters in our EPR study of $TiO_2\{001\}$, the difference of our findings in PALS and EPR should be due to the limitation of EPR, which is only sensitive to the O_V with unpaired electrons. However, both PALS and EPR studies claim that the isolated O_V disappears after Au photo-deposition, indicating that the isolated O_V should be the active site for the photo-deposition of Au.

The X-ray photoelectron spectroscopy (XPS) results (Fig. S6, ESI†) show that all Au/TiO_2 catalysts exhibit a Ti $2p_{3/2}$ binding energy at 458.7 eV and an O 1s binding energy at 530.0 eV arising from TiO_2. Meanwhile, all Au/TiO_2 catalysts exhibit a single Au 4f component with the Au $4f_{7/2}$ binding energy at 83.2–83.5 eV (Fig. 3C and D), a typical value of metallic Au supported on TiO_2.[19] Both 3% $Au/TiO_2\{100\}$, 1% $Au/TiO_2\{100\}$ and 3% $Au/TiO_2\{001\}$ with large Au nanoparticles exhibit a similar Au $4f_{7/2}$ binding energy around 83.2 eV. With a decreasing amount of Au loading and reduced size of photo-deposited Au, the Au $4f_{7/2}$ binding energy of $Au/TiO_2\{100\}$ slightly shifts to higher binding energy while the Au $4f_{7/2}$ binding energy of $Au/TiO_2\{001\}$ stays the same. It has been reported that the smaller and more dispersive nanoparticles show a higher binding energy shift compared with larger nanoparticles due to the well-known final state effects,[24] which is consistent with our finding on photo-deposited $Au/TiO_2\{100\}$ catalysts. However, no significant shift of Au $4f_{7/2}$ binding energy has been observed with reducing size and coverage of photo-deposited Au on $TiO_2\{001\}$, suggesting that the interaction between $TiO_2\{001\}$ and small Au nanoparticles could facilitate Au to obtain electrons from the adjacent $TiO_2\{001\}$ and balance the higher shift caused by final state effects. Our XPS results demonstrated that the interaction between photo-deposited Au and $TiO_2\{001\}$ should be much stronger than the interaction between photo-deposited Au and $TiO_2\{100\}$. *In situ* DRIFTS spectra of CO adsorption (Fig. S7, ESI†) were also employed to identify the types of adsorption sites on both Au and TiO_2 surfaces of various Au/TiO_2 catalysts. It is noted that the tailing peak assigned to CO adsorbed at Ti sites of $TiO_2\{001\}$ with partial negative charge at 2164 cm^{-1} disappears even after photo-depositing 0.2% Au, in agreement with our EPR findings, suggesting a direct interaction between photo-deposited Au and isolated O_V on the $TiO_2\{001\}$.

Table 1 Positron lifetimes and relative intensities of various TiO_2 and Au/TiO_2 materials

Sample	τ_1 (ps)	τ_2 (ps)	τ_3 (ps)	I_1 (%)	I_2 (%)	I_3 (%)
$TiO_2\{100\}$	194	324	NA	5.1	94.9	NA
0.2%$Au/TiO_2\{100\}$	NA	333	2737	NA	98.7	1.3
$TiO_2\{001\}$	218	340	NA	17.3	82.7	NA
0.2%$Au/TiO_2\{001\}$	NA	329	2245	NA	97.9	2.1

By applying EPR XPS and *in situ* DRIFTS to investigate the defect structures of TiO_2 nanocrystals before and after photo-depositing Au nanoparticles, we demonstrate that the isolated O_V on TiO_2 could serve as a d electron trapper and thus facilitate and stabilize small photo-deposited Au nanoparticles while the O_V clusters on TiO_2 could not directly participate in the PD process, which greatly broadens and deepens the understanding of the influence of defects in the PD process and contributes to the further design of highly efficient photo-synthesized catalysts. We herein attempted to manipulate the PD process by controlling the defect structures on TiO_2 nanocrystals. Here are some interesting findings:

Firstly, we found that both the concentration and structure of defects on TiO_2 nanocrystals can be regulated by pretreating TiO_2 nanocrystals at high temperatures. As shown in Fig. 4, the unsymmetrical F^{1+} feature of $TiO_2\{100\}$ becomes symmetric and the photoluminescence intensity dramatically decreases after treating $TiO_2\{100\}$ at 400 °C in Ar gas, indicating that the O_V cluster serves as an electron–hole recombination site while the isolated O_V acts as an electron trapper. The intensity of the symmetrical F^{1+} peak also increases after pretreating $TiO_2\{001\}$ at 300 °C in Ar gas, and the increment of the number of isolated O_V could facilitate dispersive photo-deposited Au (Fig. S8, ESI†). The average sizes of photo-deposited Au are 25.5 ± 9.7, 10.3 ± 4.3, 6.6 ± 1.9 and 5.4 ± 1.9 nm in 1% $Au/TiO_2\{100\}$, 1% $Au/TiO_2\{100\}$-400Ar, 1% $Au/TiO_2\{001\}$ and 1% $Au/TiO_2\{001\}$-300Ar, respectively, and the intensities of all symmetrical F^{1+} peaks dramatically decrease after Au photo-deposition.

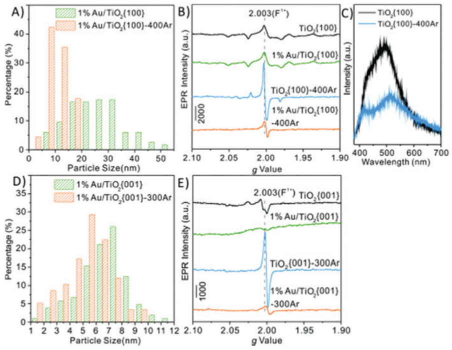

Fig. 4 (A and D) Au nanoparticle size distributions of various 1% Au/TiO_2 materials, (B and E) EPR spectra of various TiO_2 and 1% Au/TiO_2 materials, and (C) PL spectra of TiO_2{100} and TiO_2{100}-400Ar nanocrystals.

Secondly, we found that the influence of defect structures on photo-deposited Au is suitable for other photo-deposited metals, such as Ag and Pt. Both Ag/TiO_2 and Pt/TiO_2 catalysts with calculated 1% metal/TiO_2 weight ratio were prepared following a similar procedure as photo-deposited Au by employing TiO_2{100} and TiO_2{001} as supports. Fig. S9 and S10 (ESI†) displays images and metal nanoparticle size distributions of these catalysts. The average Ag and Pt nanoparticle sizes are 22.2 ± 6.6, 3.8 ± 2.6, 4.3 ± 1.9 and 2.3 ± 0.8 nm in 1% Ag/TiO_2{100}, 1% Ag/TiO_2{001}, 1% Pt/TiO_2{100} and 1% Pt/TiO_2{001}, respectively. These results demonstrate that TiO_2{001} can facilitate and stabilize dispersive photo-deposited Ag and Pt nanoparticles compared with TiO_2{100}, which is consistent with our finding on photo-deposited Au nanoparticles.

By controlling the intensity and structure of defects on TiO_2 nanocrystals, we have successfully synthesized photo-deposited Au nanoparticles with designed size distribution. The average Au nanoparticle sizes are 25.5 ± 9.7, 10.3 ± 4.3, and 6.6 ± 1.9 nm in 1% Au/TiO_2{100}, 1% Au/TiO_2{100}-400Ar and 1% Au/TiO_2{001}. Photocatalytic water reduction was employed to evaluate the catalytic activity of these photo-deposited Au/TiO_2 catalysts (Fig. S11, ESI†). The H_2 evolution rates of bare TiO_2{100} and TiO_2{001} nanocrystals are negligible, and the H_2 production rates are 0.83 ± 0.04, 1.2 ± 0.08 and 1.6 ± 0.04 mmolH_2 g^{-1} h^{-1} for 1% Au/TiO_2{100}, 1% Au/TiO_2{100}-400Ar and 1% Au/TiO_2{001}, respectively. It is expected that 1% Au/TiO_2{001} with the smallest size of photo-deposited Au nanoparticles exhibits the best catalytic performance of water reduction.

In conclusion, the influence of defect structures on the photo-deposited metal nanoparticles has been systematically studied in our study. We demonstrate that the isolated O_V could serve as an electron trapper and facilitate the formation of small photo-deposited metal nanoparticles while the O_V clusters act as electron–hole recombination sites in the PD process and only result in large metal nanoparticles. We further found that both the intensities and the structures of defects can be controlled by pre-treating TiO_2 at high temperature, which provides us with a great opportunity to synthesize photo-deposited metal nanoparticles with optimized size distribution and catalytic performance. Our findings would greatly broaden and deepen the understanding of the influence of defect photo-generated charge separation and shed light on controllable synthesis of highly efficient active structures.

This work was financially supported by the National Key R&D Program of the Ministry of Science and Technology of China (2017YFB0602205), the Fundamental Research Funds for the Central Universities (WK2060030030), the National Natural Science Foundation of China (21872128, 21525313, 91745202, and 21703001), the Anhui Provincial Natural Scientific Foundation project (1808085MB44), the Chinese Academy of Sciences, and the Changjiang Scholars Program of Ministry of Education of China.

Conflicts of interest

There are no conflicts to declare.

Notes and references

1 X. L. Jiang, X. L. Fu, L. Zhang, S. Menga and S. F. Chen, *J. Mater. Chem. A*, 2015, **3**, 2271–2282.
2 A. Kudo and Y. Miseki, *Chem. Soc. Rev.*, 2009, **38**, 253–278.
3 K. Maeda, *J. Photochem. Photobiol., C*, 2011, **12**, 237–268.
4 S. C. Roy, O. K. Varghese, M. Paulose and C. A. Grimes, *ACS Nano*, 2010, **4**, 1259–1278.
5 J. Zhao and X. Yang, *Build. Environ.*, 2003, **38**, 645–654.
6 B. Kraeutler and A. J. Bard, *J. Am. Chem. Soc.*, 1978, **100**, 4317–4318.
7 P. X. Liu, Y. Zhao, R. X. Qin, S. G. Mo, G. X. Chen and N. F. Zheng, *Science*, 2016, **352**, 797–801.
8 S. C. Chan and M. A. Barteau, *Langmuir*, 2005, **21**, 5588–5595.
9 R. G. Li, F. X. Zhang, D. E. Wang, J. X. Yang, M. R. Li, J. Zhu, X. Zhou, H. X. Han and C. Li, *Nat. Commun.*, 2013, **4**, 1432–1438.
10 S. Y. Wang, Y. Y. Gao, S. Miao, T. F. Liu, L. C. Mu, R. G. Li, F. T. Fan and C. Li, *J. Am. Chem. Soc.*, 2017, **139**, 11771–11778.
11 K. Teramura, S. Okuoka, S. Yamazoe, K. Kato, T. Shishido and T. Tanaka, *J. Phys. Chem. C*, 2008, **112**, 8495–8498.
12 F. Forouzan, T. C. Richards and A. J. Bard, *J. Phys. Chem.*, 1996, **100**, 18123–18127.
13 J. M. Herrmann, J. Disdier and P. Pichat, *J. Catal.*, 1988, **113**, 72–81.
14 K. Wenderich and G. Mul, *Chem. Rev.*, 2016, **116**, 14587–14619.
15 A. L. Linsebigler, G. Q. Lu and J. T. Yates Jr, *Chem. Rev.*, 1995, **95**, 735–758.
16 M. Zhang, Z. S. Jin, J. W. Zhang, X. Y. Guo, J. J. Yang, W. Li, X. D. Wang and Z. J. Zhang, *J. Mol. Catal. A: Chem.*, 2004, **217**, 203–210.
17 S. L. Chen, T. Cao, Y. X. Gao, D. Li, F. Xiong and W. X. Huang, *J. Phys. Chem. C*, 2016, **120**, 21472–21485.
18 S. L. Chen, D. Li, Y. X. Liu and W. X. Huang, *J. Catal.*, 2016, **341**, 126–135.
19 S. L. Chen, B. S. Zhang, D. S. Su and W. X. Huang, *ChemCatChem*, 2015, **7**, 3290–3298.
20 D. Li, R. You, M. Yang, Y. X. Liu, K. Qian, S. L. Chen, T. Cao, Z. H. Zhang, J. Tian and W. X. Huang, *J. Phys. Chem. C*, 2019, **123**, 10367–10376.
21 C. P. Kumar, N. O. Gopal, T. C. Wang, M.-S. Wong and S. C. Ke, *J. Phys. Chem. B*, 2006, **110**, 5223–5229.
22 M. Fittipaldi, D. Gatteschi and P. Fornasiero, *Catal. Today*, 2013, **206**, 2–11.
23 M. Su, *Solid State Chemistry: An Introduction*, Peking University Press, Beijing, 1987 (in Chinese).
24 G. K. Wertheim and S. B. DiCenzo, *Phys. Rev. B: Condens. Matter Mater. Phys.*, 1988, **37**, 844–847.
25 S. J. Chang, M. Li, Q. Hua, L. J. Zhang, Y. S. Ma, B. J. Ye and W. X. Huang, *J. Catal.*, 2012, **293**, 195–204.
26 A. Fu, X. Chen, L. H. Tong, D. F. Wang, L. Q. Liu and J. H. Ye, *ACS Appl. Mater. Interfaces*, 2019, **11**, 24154–24163.